On the Necessity and Feasibility of an Equatorial Magnetospheric Constellation

V. Angelopoulos, C. W. Carlson, D. W. Curtis, P. Harvey, R. P. Lin, F. S. Mozer, D. H. Pankow

Space Sciences Laboratory, University of California, Berkeley, CA

J. Raeder, C. T. Russell

Institute of Geophysics and Planetary Physics, University of California, Los Angeles, CA

Abstract. Synthesizing multi-point in-situ observations from the magnetosphere is the only way that we can retain an accurate knowledge of the driving mechanisms of convection and energy flow while "imaging" its vast volume. In addition to measuring the wavenumber of plasma instabilities thus opening up for study a previously unexplored domain of space plasma physics the Constellation mission can afford us a view of the rapid topological reconfigurations and the energy circulation throughout the astrophysical laboratory closest to human space activity. In this paper we argue that the deployment of ~80 autonomous micro-satellites (probes) to monitor the Earth's magnetosphere and measure the plasma and magnetic field in the near-equatorial magnetosphere is a necessary and sufficient condition for answering long standing, high priority questions regarding magnetospheric stability and dynamics. The proposed mission concept is technically feasible and fiscally modest. The probes can be raised from a Geosynchronous Transfer orbit to their final elliptical orbits with perigee ~3 R_E and apogees ranging from 12 to 42 R_E by a single dispenser propelled by an ion engine. Each probe will weigh ~5 kg. The mission can form a cornerstone of an incrementally deployed Solar Terrestrial Probe Line Magnetospheric Constellation, as it requires no new technologies in the areas of spacecraft subsystems and instruments, but some development in the areas of dispenser design, probe packaging, mechanical release and spin-up. The technology developed can be utilized by follow-on Constellation class missions as well.

1. Introduction

The long term correlation between isolated measurements in separate geophysical regions (the solar wind, the magnetotail, the ionosphere, and the polar cap) will be obtained by ISTP, putting to test on gross spatial and temporal scales our current theories and models of magnetospheric evolution. As we arrive at deeper levels of understanding of each geophysical region, we realize that spatio-temporal ambiguities riddle our interpretations of single-point measurements from that region. Simultaneous fortuitous spacecraft conjunctions within the same magnetospheric region exist in the ISTP era, but those are limited to, at most, three spacecraft at a time and have interspacecraft separations that are not optimal for single region studies. Consequently, ISTP spacecraft are also subject to the interpretational ambiguities common to single-spacecraft missions.

The ESA/NASA mission CLUSTER and the Solar Terrestrial Probes mission Magnetospheric Multiscale (MM) on the other hand, will provide a much improved perspective of the microphysics of magnetospheric phenomena. They promise to measure currents routinely and to resolve spatio-temporal ambiguities around a localized part of each region. They are primarily designed to study sharp boundaries and thus their inter-satellite separation will not exceed ~2 R_E.

Approved missions to globally monitor the magnetosphere are IMAGE and TWINS. Imaging the tenuous magnetotail plasma with current energetic neutral atom or other imaging techniques is not possible at the short time scales of approximately a minute during which the system reconfigures. Thus, although IMAGE and TWINS will provide unprecedented information at the day side magnetosphere and the near-Earth environment, similar information from the magnetotail will be lacking. Yet, it is in the magnetotail where the solar wind energy transforms into kinetic and thermal plasma energy that then affects the near-Earth environment. The multi-point study of that energy transformation and the associated configurational changes in the magnetosphere are primary goals of space physics today [*Angelopoulos and Spence*, 1998]. Although our ultimate goal is to pixelize the entire magnetospheric system in a science-driven fashion, our approach in this paper will be to start by identifying the most essential questions that need to be answered in the field of magnetospheric research, perform a feasibility analysis of a strawman mission concept, and pinpoint the elements that render this minimal mission possible.

2. Zero Level Science Goals

Of all the questions in magnetospheric physics, one has accompanied the historical evolution of the field over the last 30 years, yet still remains largely unresolved: That of conversion of magnetic to plasma kinetic and thermal energy during the course of magnetospheric substorms and the associated magnetospheric reconfiguration. Knowledge accumulated to date strongly indicates that the difficulty lies in the localization of the phenomena both in space (to scale sizes of 1-2 R_E) and in time (1-2 minutes) despite their large-scale consequences over longer time scales. A single spacecraft within the vast magnetospheric system has little chance of being at the key regions at the time of substorm onset. More importantly, the lack of simultaneous measurements from adjacent "pixels" of the system prohibits us from placing the observed phenomenon in the context of the global magnetotail evolution. In the following, we present the zero level questions and document the necessity for a multi-probe investigation of the magnetotail.

2.1 Substorm Chronology

Substorms are defined on the basis of their ionospheric signatures [*Rostoker et al.*, 1980] but they have repeatable near-Earth magnetospheric signatures. These are: the energization of particles at geosynchronous altitude and the elevation increase of the magnetic field in the near-Earth nightside magnetosphere [*McPherron et al.*, 1991]. Contrary to the ionosphere, where a global picture can be obtained with all-sky cameras, radars, and magnetometer networks, in space we depend on statistical analyses to compose a time history of events. Such analyses and a few fortuitous two- or three-spacecraft conjunctions, we have learned that the field dipolarization starts at a localized region of the order of 1-2 R_E [*Ohtani et al.*, 1992] and propagates longitudinally [*Nagai*, 1982] at a speed of an hour of local time every 1-3 minutes and radially tailward [*Jacquey et al.*, 1993] with a speed of ~250 km/s, or 2.5 R_E/min. Tailward flows are also observed during substorms,

Science Closure and Enabling Technologies for Constellation Class Missions, edited by V. Angelopoulos and P. V. Panetta, pp.14-21, UC Berkeley, Calif., 1998.

most often at distances greater than 19 R_E, while Earthward flows are observed closer to Earth [*Angelopoulos et al.*, 1994]. These flows have been interpreted as signatures of magnetic reconnection. The reconnection site also moves downtail during the course of a substorm [*Sergeev et al.*, 1995] at speeds comparable to the speed of the current disruption.

The time and location of the first magnetospheric signature of substorm onset and its relationship with the ground observables still remains a mystery. For example, Baker and McPherron [1990] suggest, on the basis of the near-Earth neutral line model, that tailward flows should start before ground substorm onset. However, Lui [1996] suggests on the basis of the current disruption model that tailward flows are the consequence of near-Earth current disruption and thus reconnection should then start after substorm expansion phase onset. The "strong version" of the Kiruna conjecture [*Kennel*, 1992] has been that not only this remains an open question but that there is also the possibility that the two phenomena are entirely uncorrelated. The resolution of this issue requires sufficient (less than 1 minute, the Alfven bounce time) temporal resolution and sufficient (~1-3 R_E, the scale size of the initial active region) spatial plasma sheet coverage on the X-Y plane.

The maximum altitude of spacecraft necessary to capture the reconnection process is determined from recent GEOTAIL results, which place the most likely position of the near-Earth neutral line at around X=-20 to -25 R_E [*Nagai et al.*, 1997]. Many tens of spacecraft at cross-tail separations ranging between 1 and 20 R_E and at downtail positions between 7 to 40 R_E are a sufficient condition for the study of the magnetospheric evolution during the course of a substorm. Quantities necessary and sufficient are high time resolution (1-5 s) magnetic field and 3D ion moment measurements.

2.2 Substorm Current, Energy and Magnetic Flux Budgets

Substorms are the primary mechanism of energization of the nightside ionosphere and ring current. Modeling of the geosynchronous injections during substorms as fronts of Earthward-collapsing particles [*Mauk*, 1986] based on measured electric fields observed in the near-Earth plasma sheet [*Aggson et al.*, 1983; *Maynard et al.*, 1996] has produced fairly good agreement between theory and observations [*Quinn and Southwood*, 1982]. In that scenario it is the braking of the Earthward flows [*Shiokawa et al.*, 1998] resulting from either the current disruption or the reconnection process that causes the near-Earth signatures of substorms. In the magnetotail tailward of X=-15 R_E, and close to the neutral sheet, fast plasma sheet flows are responsible for most of the plasma sheet energy, particle and flux transport [*Angelopoulos et al.*, 1994]. Such flows are most often observed within |Y|<5 R_E from the midtail axis [*Baumjohann et al.*, 1990]. Are the fast flows that are observed at substorm onset of sufficient energy to account for substorm energization of the near-Earth environment and the ionosphere? The answer depends on the 3D evolution of the magnetotail flows. Given the extreme localization in Y of some of the fast flow events observed so far, simultaneous multi-point measurements over an extent of $\Delta Y \sim 10\ R_E$ and at a probe density of 1 measurement per 1-3 R_E in Y are necessary.

The longitudinal spread of the substorm current wedge (SCW) is coupled to the westward traveling surge in the ionosphere [*Roux et al.*, 1991; *Robert et al.*, 1984; *Maynard et al.*, 1996]. The extent in Y of the SCW at distances far from geosynchronous is neither known, nor possible to document with single spacecraft because it is a three dimensional system. Lopez and Lui [1990] used AMPTE/IRM and CCE observations to show that the SCW is irregular in space. Moreover, substorms typically manifest themselves as a series of consecutive, isolated activations. The near-Earth and ground signatures are the integral response to multiple localized acceleration sites. Such individual activations are possibly the elemental processes comprising substorms [*Sergeev et al.*, 1986]. Multi-spacecraft observations will result in resolving the ambiguities associated with the number, location and extent of such activations. Understanding the three-dimensional evolution of the substorm current wedge system promises to solidify estimates of the magnetospheric-ionospheric energy coupling during a substorm.

2.3 Current Sheet Thickness and Evolution.

Present theories attempting to address the substorm onset question on the basis of current sheet instabilities require direct measurements of the current sheet thickness and intensity [*Lui*, 1996]. Attempts to model the current sheet thickness and density by inverting the observed magnetic field measured at more than one locations during fortuitous conjunctions of spacecraft has lead to considerable success [*Pulkkinen et al.*, 1991]. In addition, inversion techniques in the tail using two spacecraft [*McComas et al.*, 1986] have given incontrovertible evidence of the existence of thin current sheets and their importance during substorms [*Lin et al.*, 1991]. However, the only possible way to ensure that the tail current system is adequately monitored at the time and place where it actually becomes unstable is to simultaneously monitor its thickness at many different downtail distances. This necessitates a CLUSTER-like system at many different distances. One way to achieve that is to provide some orbits with enough separation in Z (~1-2 R_E) at different downtail distances. For current sheet densities of the order of 1 nA/m^2 which are typical of the cross tail current, and inter-satellite separations of 1 R_E such measurements can be made comfortably with 0.5 nT accuracy i.e. well within the capabilities of conventional magnetometer designs. Vertical separations of the order of 1 R_E are necessary in order to bracket the thin and often variable-scale-size cross tail current but also sufficient for such observations.

2.4 Modeling and Variability of Magnetospheric Currents

Global magnetospheric models, with the exception of global MHD are static [*Tsyganenko*, 1995]. The large magnetic field variability in the databases that are used as input to those models [*Stern and Tsyganenko*, 1992] suggest that a significant part of the physics that determines the most probable magnetospheric state is missed. Most often, severe modification of the model currents is necessary away from expected state [i.e., for the measured Kp or AE parameter] when actual time-dependent situations are considered [*Pulkkinen*, 1991]. It is impossible for a static model parametrized on global indices to capture the complexity, the richness and the physics of the instantaneous magnetospheric configuration. However, a large array of measurements from magnetospheric probes can produce, when inverted using techniques available from statistical [*Tsyganenko and Usmanov*, 1982], simulation [*Berchem et al.*, 1995] and atmospheric [*Ghil and Malanotte-Rizzoli*, 1991] models, an instantaneous "image" of currents and fields that is consistent with the average tail structure but representative of the instantaneous measured fields. This can produce a far clearer picture of the current systems' sources, sinks and temporal evolution.

2.5 Fate of Accelerated Particles

The three-dimensional circulation of the substorm-accelerated particles is not clearly understood. Huang et al. [1992] have shown that plasma sheet temperature increases after substorm onset represent an important plasma sheet response to geomagnetic activity that does not

always correlate with flow enhancements. Although single particle approaches [*Spence and Kivelson*, 1993; *Spence et al.*, 1993; *Ashour-Abdalla et al.*, 1994] have led to certain predictive pictures of the plasma sheet pressure, temperature and density spatial profiles, which have yet to be verified observationally. There is a clear need to observe the system and its evolution at many points simultaneously for a given thermodynamic state. This entails fine spatial resolution observations of the instantaneous flow pattern, density and temperature to observe the source and propagation of the resulting heating. The reason for the fine spatial resolution is twofold: First, the acceleration regions are localized in space [*Angelopoulos et al.*, 1997]. Second, the plasma sheet flow and thus particle trajectories are variable at inferred spatial scales of ~2 R_E, such that it is unlikely that two spacecraft will have many chances of crossing the same flow line at a given time. A large enough probe density and high-time (~5 s) resolution distribution functions are necessary to resolve this problem. Thus burst-mode operations at times of substorm onset must be provided by the zero level mission.

2.6 The Most Common State of the Plasma Sheet

Although the most dramatic plasma sheet phenomena occur during short periods, at a good statistical correlation with substorm activity, the most probable state of the plasma sheet (90-95% of the time) is the non-flowing state [*Baumjohann et al.*, 1989]. That state exhibits flows in any direction with equal probability and with a peak-to-peak amplitude may times larger than the average flow itself [*Angelopoulos et al.*, 1993]. Despite the large flow variability, the average flow pattern exhibits behavior that can be understood in simple 2-fluid theory [*Angelopoulos et al.*, 1993] or single particle orbits [*Spence et al.*, 1993a, 1993b]. Significant variability about the magnetic field average also exists [*Stern and Tsyganenko*, 1992], rendering orbit integration schemes vulnerable to criticism. Is the variability the consequence of nearby high speed flows or the result of complex ion trajectories under steady external conditions? Velocity autocorrelation times are of the order of 2-3 minutes and mixing lengths of the order of 1-2 R_E [*Borovsky et al.*, 1997]. In order to characterize this state of the plasma sheet correlative measurements that measure the wavelength spectrum of the plasma sheet flows are necessary. This will tell us if the variability is generated by the substorm process of it is an inherent property of the convecting plasma sheet. Distribution functions are necessary in order to ascertain whether the flow variability is due to particle bunching or a velocity shift of the entire particle distribution. As the time scale of propagation of an ion of 1 keV energy is ~4 R_E/min we can monitor the propagation of such ions between satellites separated by a distance of 10 R_E within 2 minutes. Thus, it is important to operate at a burst mode of collection of distribution functions from all spacecraft during periods of 2-10 minutes, even outside of substorm onset intervals.

2.7 Plasma Sheet Thermodynamics

Attempts to characterize the thermodynamics of the plasma sheet (such as measuring its polytropic index) have been so far inconclusive [*Baumjohann and Paschmann*, 1989; *Huang et al.*, 1989; *Goertz and Baumjohann*, 1991]. Room for controversy exists because with single spacecraft we cannot observe the evolution of a single flux tube. Multi-probe studies that utilize two (or more) spacecraft traversing plasma streamlines will be able to answer the above question. However, such studies may result in a complete change of mindset regarding this issue, since if the plasma flow is non-laminar the concept of a streamline may be invalid.

3. The Zero Level Mission

3.1 Overview

The zero level science goals can be met with a fleet of 80 low-cost, low-data-rate probes identically instrumented with a triaxial fluxgate magnetometer and a three-dimensional ion distribution sensor. The probes will be spin stabilized at a period of 3 s. The number of probes was chosen based on a science-driven plasma sheet coverage of 1 probe per ~3 R_E^2 covering the region -10<X<-40 R_E and -5<Y<5 R_E and assuming an equatorial distribution of probes that is randomized due to orbital perturbations. Low data accumulation rates will result in low transmission power requirements at perigee (store-and-dump downlink). Perigee will be between 2.5 and 3.5 R_E, to ensure an acceptable transmission rate, adequate visibility from two antidiametrically located ground tracking stations and a relatively benign proton radiation environment. The probes can be stacked in a single dispenser released by the launch vehicle on a Geosynchronous Transfer Orbit (GTO). The dispenser can be 3-axis stabilized and be propelled by an ion engine. It will carry the payload from GTO (185X45000 km altitude) to the highest semimajor axis final orbit (3X42 R_E geocentric). It should release the probes, one at a time, along its ascend to the final orbit. A Taurus XLS (4213) with two Castor 4B strap-ons (Med-Lite configuration) can deliver 590 kg to the above GTO orbit for a cost of $30 M. Assuming a 1.25 kW power (single solar array) input to the ion engine, the dispenser can release all the probes within 80 days.

3.2 Orbit Characteristics

The orbits were chosen on the basis of the following requirements: 1) The orbits should have a maximal probability of being inside the plasma sheet, if not at the neutral sheet. Since the distortion of the neutral sheet surface increases with dipole tilt, we demand that the apogees be at midnight at equinox, a period associated with minimal seasonal tilt. 2) The orbit planes should cross the neutral sheet at times when ground magnetometer and radar coverage is maximal, i.e. when the US sector is near midnight (i.e., at 0630 UT). At that time and at vernal equinox the dipole tilt is approximately -10 degrees. 3) The orbits should avoid Earth's shadow for periods longer than 1-2 hours to avoid complex thermal and electrostatic designs. 4) Every 5 R_E in apogee distance, two probes should be released so as to be separated by a constant Z-separation (~1 R_E) at apogee. These probes will be utilized to measure the cross tail current and its thickness. The resulting orbital distribution is shown in Figure 1.

For demonstration purposes the probes were placed at their perigee at the same time (Winter Solstice, 1996) and then were propagated using the Goddard Trajectory Determination System (includes Solar, J2, Lunar and atmospheric perturbations) to their positions 3 months later. Sufficient longitudinal coverage and sufficient probe density is achieved, in accordance with the science requirements. Figure 6 of Delory *et al.* [1998] shows that the Z-separated probes are not significantly affected by orbital perturbations for a period of more than 1 year and possibly longer than that.

Three months of data collection in the magnetotail will have completed the basic mission science objectives within 8 months from launch, i.e., including 5 months for achieving the final orbit, instrument checkout and inter-calibration. Furthermore, in accordance with the principles of an incremental deployment of a constellation mission, the equatorial probes can enhance significantly other Constellation class missions that will follow. It is prudent to ensure a prolonged (>1 year) lifetime in terms of parts quality, radiation hardness, and solar cell, battery and instrument lifetimes. The prolonged lifetime should not be

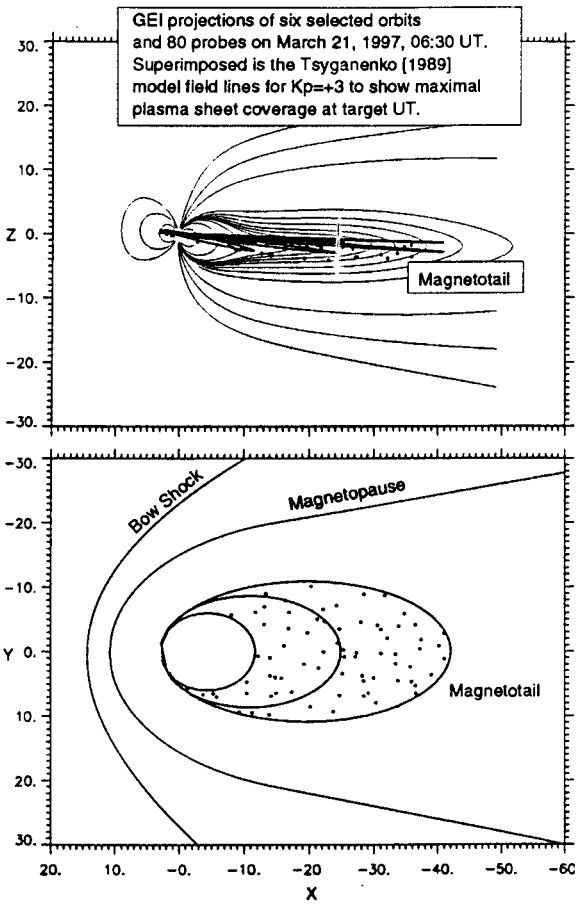

Figure 1. Zero level mission orbits.

a requirement but a desire, in order to not escalate mission costs beyond feasibility for a Med-Lite launcher and a MIDEX class mission cost. A probe loss of even 30% of the probes can be tolerated in the phase of follow-on Constellation mission support.

3.3 Instruments

Magnetic field measurements at 1-5 s resolution with spin axis and angle knowledge of ~0.1 degrees, sensitivity of ~0.1 nT and range from 0-2000nT are required. An orthogonal triad of sensors on a fixed boom (30 cm) is far enough from the spacecraft that does not necessitate an expensive magnetic cleanliness program, especially with an early design and problem mitigation program. Wiring of solar cells, battery and instruments are the most important items in such a program, but are quite benign relative to subsystems on traditional spacecraft. The electronic design can be borrowed from that used on the FAST Small Explorer mission with small simplifications for reducing power and weight. The modifications should take advantage of relaxed reliability requirements stemming from redundancy that is built in the numbers of probes rather than in the probe components. The mass of the main electronics is 0.4 kg and the sensor triad plus cabling is 0.1 kg. The electronics unit draws 0.5 W of refined power. By minimizing range changes and using digital filters, the magnetometer is both simple to calibrate on the ground and easy to operate in space. On board spin averaging can be performed with a simple hardware-implemented addition and subtraction operation using the sun pulse as reference at a negligible power cost. The magnetometer boom structure, be it of a telescopic or hinged arm type, weighs less than 100 grams including wiring.

Table 1. Science Payload and data accumulation

INSTRUMENT	Mass	Power	Data Rate†	Data (bits/Orbit)‡
Triaxial Fluxgate Magnetometer	0.6 kg	0.5 W	17 bps	$1.0X10^7$
Ion Electrostatic Analyzer: Top hat, 180^o X 22.5^o FOV; 16 Energies, 3eV-40keV	1.0 kg	0.75 W		
Moments.....			35 bps	$2.0\ 10^7$
f(v)@ 5 min.....			30 bps	$1.7\ 10^7$
Burst:20 min @ 6 s.			3.2 10^6 bits/day	$2.1\ 10^7$
TOTAL	1.6 kg	1.25 W		$6.8\ 10^7$

†Assuming a 3s spin period.
‡Assuming the highest apogee orbit (period ~6.5 days).

A top-hat ion electrostatic analyzer with a heritage from FAST will perform measurements of ions in the 3 eV - 40 keV range. The configuration has a 180X14 degrees field of view allowing measurement of a full 3D distribution function once per spin. Ions entering the analyzer are selected in energy and imaged onto a microchannel (MCP) plate at 8 separate angles. Using a 20% margin on total power we get power consumption less than 750 mW. Measurements are performed at 16 energy steps with width $\Delta E/E=0.78$ and a geometric factor of $4x10^{-2}$ cm^2-sr-eV. Raw data in a full distribution function is 16384 bits. This is fed to the data processing unit which performs the moment computations. The basic quantities of density, velocity, and pressure tensor give us ~104 bits per measurement.

The probe design is such that cannot afford multiple subsystems bolted on a generic bus. Bus design must be "holistic" i.e., instruments and spacecraft subsystems must be highly integrated (Figure 2). The probe must be viewed as a single instrument, minimizing connectors, wires and integration and testing. A triangular shape provides minimal spin-ripple of solar input power.

3.4 Data Acquisition

Following the science requirements from the previous section we assume magnetic field and ion moments collection at 3s resolution (1 spin). Routine transmission of ion distributions is necessary every ~5 minutes for ascertaining the validity of the on-board ion moment computations, and studying individual events in detail. Burst mode storage of ion distributions is necessary when most satellites are positioned in the plasma sheet at a high rate (6 s) for a period of ~20 minutes/day. This mode can be routinely performed at times that the expected neutral sheet crossings occur on the basis of a model, upon ground commands, or upon an on-board-detection of an "active" plasma sheet encounter. The total data budget for the mission is shown in Table 1. A total of 68 Mbits will be stored in the highest apogee orbit, (6.5 days) including burst mode data. Data compression can further reduce the total amount of data significantly allowing either higher sampling rates or increased burst time.

3.5 Data Storage

Data storage requires a maximum of 80 solid state memory chips (SRAM, 1 Mbit each) at a total of 160 grams including a hardware-

implemented, error-correcting code. Moment computations, data compression and signal conditioning can be done on the Data Processing Unit (DPU). This is composed of 2 programmable gate array chips at a total weight of 10 grams and a central computational unit of 50 grams. Additional computations performed are instrument control, command and data transfers to sensor electronics, data packetizing, CCSDS telemetry formatting, Viterbi R1/2 telemetry encoding and power control. An additional 100 grams for the board results in a total memory plus DPU weight of less than 250 grams. The power required for the memory is 0.2 Watts based on FAST technology, while the DPU power consumption based on the components above is 0.1 W. New technologies from the commercial sector can result in further DPU mass and power reduction.

3.6 Data Transmission

Data transmission can be achieved at or near perigee (3 R_E perigee, or ~13000 km minimum range). Assuming contacts from a range of 20,000 km or less, an omnidirectional transmitter in the S-band (2.3 GHz) with radiated power of 2 Watts, and a 10 m diameter ground station, we can achieve a downlink rate of 200 kbps, with link margin better than 5 dB (see *Angelopoulos et al.*, 1998 for the details of the link computation). The telemetry system envisioned comprises a body-mounted whip 1/4 wave antenna. The antenna gain pattern is subject to diffraction and is quite isotropic [*Yuriev et al.*, 1998]. The total antenna weight is approximately 50 grams. The transmitter can operate at 28V voltage and is drawing 0.8A maximum current with 2 Watts output power. Even in the absence of data compression the total time required for data transmission is less than 6 minutes. This requires a total energy of ~2.5 Wh which has to be supplied by the battery. The commercial receiver envisioned operates using the same antenna in a slightly different frequency. There is no requirement for two-way communications, which makes for a simple RF system on-board.

3.7 Power

Powering transmitters with a nominal 10% efficiency using conventional Cadmium batteries would be exceedingly heavy for the mission. We sought alternative solutions in Li-Metal (LiM) and Nickel-Metal-Hydrate (NiMH) battery technologies, which are driven by the cellular telephony industry. As an example the rechargeable AA size Lithium battery type TLR-7103 manufactured by Tadiran can operate nominally at 2.8 V and draw 250 mA of current. It can operate in the range -30 to 55 degrees Celsius and provide 500 cycles of charge/discharge operations at 50% depth of discharge (DOD). It weighs 17 grams. As we need 28 Volts and 0.8 Amps for nominal transmitter operation we need to stack 10 such batteries in series and have three stacks (30 cells total) of a total weight of 510 grams. The nominal battery capacity is 0.75 mAh. This gives us a total of 63 Wh. Operating at DOD of 4% we can achieve the transmitter requirement of 2.5 Wh at a comfortable margin to allow for battery degradation or partial cell failure. Given one battery discharge (data transmission) per ~6 days this allows a lifetime of 3000 days, i.e. much longer than the mission lifetime. An alternative scenario that doubles the DOD to 8% but provides two identical stacks of batteries for redundancy is also possible. Usage of NiMH battery technology (instead of LiM) can result in similar power system capabilities.

The batteries are powered by solar cells. We can use flat square panels of 6 inch side, made up of 2cm X 2cm -size GaAs cells. Each panel can produce at the end-of-mission (1 year duration assumed) a power of 3.2 Watts and 32.5 Volts, in the fluences expected in the lowest (heaviest radiation) orbit. With 6 mils of coverglass used in the

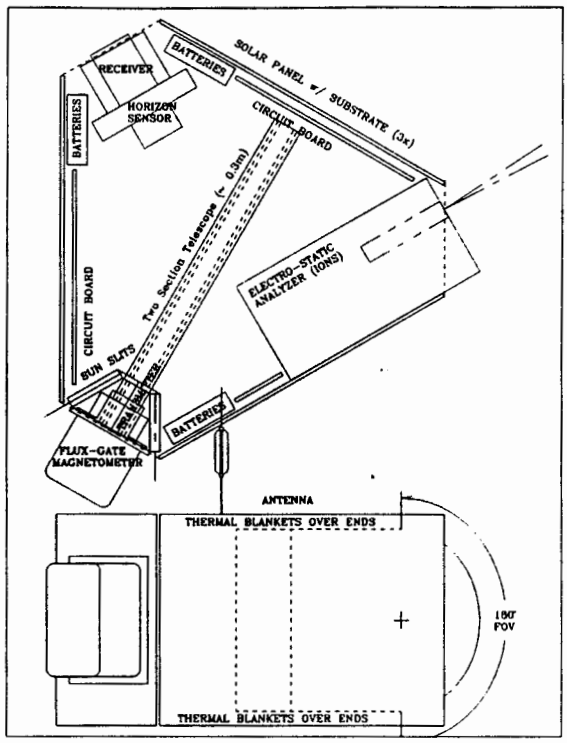

Figure 2. Payload layout.

above computation, 19% of the solar cell weight is in the coating, 40% is in the cell itself and the remainder of the weight is in the adhesive, wires and other circuitry. Each panel weighs 38.4 grams. A nearly-constant power of 3.2 Watts is thus produced during a spin. The end-of-mission characteristics satisfy the power needs of 2.834 W at a weight (3 panels) of 0.115 kg. The panels should be mounted on a graphite epoxy substrates of thickness 0.5 mm weighing less than 75 grams, including mounting posts on the spacecraft body.

3.8 Tracking

Assuming a random set of orbits with perigee at 3 R_E and apogees ranging from 12 to 42 R_E, how many can we track within a given period of ~6.5 days (longest period orbit)? We performed a simulation of the above question after launching the spacecraft from perigee on March 21, 1997, allowing two months for orbit randomization. Figure 11 of Angelopoulos et al. [1998] shows in open boxes the times that a probe was tracked by the 11 m antenna at UC Berkeley versus the probe number (probe number is assigned according to apogee in ascending order). Only 60 probes were used in the plot but the coverage results can be readily extended to 80 probes since the probes used cover the same range of apogees i.e., from 12 to 42 R_E. This is essentially a ground station tracking schedule for an arbitrary 6.5 day-period in the life of the mission. A successful probe contact constitutes a 30 min tracking opportunity (probe visibility 10 degrees above the horizon) for the purposes of that plot. The extra time above 6 m minutes of contact time is allocated for ensuring troubleshooting in cases of problem, but is not allocated routinely. A 10 minute tracking window is assumed for cost estimation purposes. With a single station we were able to track 77% of the probes. Probes that were not tracked by the UC Berkeley station were predominantly those that did not make ground contact over the 6.5 day period, not ones lost due to schedule conflicts.

These are mostly the highest apogee orbits (6 day period) because those orbits only had one chance for contact at perigee, during which time the ground station happened to be at the wrong local time. The remaining 23% of the orbits not tracked by UCB can be tracked from a station approximately 180° longitude away from UCB, such as Malindi, Kenya (currently operated by ESA). By using station Malindi to track the remaining probes we were able to retrieve more than 95% of the data. This is a satisfactory data retrieval rate for the mission envisioned. We conclude that 2 ground stations can achieve the mission objectives.

3.9 Ground Operations

Simple probes do not necessitate complex ground operations. Ground station automation as it is currently applied on Small Explorer missions can drastically reduce mission operations costs to far below the current norm of $400/contact. Some aspects of the ground operations are outlined in Angelopoulos et al. [1998].

3.10 Attitude and Orbit Determination

The ACS requirements are quite simple. Only attitude knowledge to within 0.5 degrees is required. This attitude knowledge can be achieved from a combination of two sun sensors on a V-shaped slit and an infrared detector for Earth and Moon detection. Error analysis of typical, low cost, light weight sensor data result in a 3-sigma error of less than 0.5 degrees.

Orbit determination to better than 600 km at apogee is the science requirement. This results in interprobe separation knowledge to within 10% or better. This can be easily achieved from ground station angles obtained from tracking. The orbit solution converges. Given the long (2 month) period that intervenes between the probe release and the commencement of the primary science phase of the mission, there is adequate time for solution convergence of all orbits, including the highest apogee ones.

3.11 Probe Mass and Power Summary

Table 2 presents the mass and power estimates of the proposed probe design. In addition to the power estimates described in the individual sections above, we note the following: the command receiver will be turned off in the data collection phase but in the event of malfunction it will be in the "ON" mode. We thus include it in the power budget with a pulsed, 10% duty cycle. The transmitter can operate once per ~6 days (once per six orbits for low apogee orbits or once per orbit for high apogee probes) and will draw 2.5 Wh of energy from the battery. Recharge will take place in 6 hours drawing 0.62 W solar power.

Table 2. Probe mass and power summary.

ITEM	WEIGHT	POWER (Duty Cycle)
POWER SUBSYSTEM	0.810 kg	Battery: 0.62 W (6-hr battery recharge with 2.5 Wh) Inverter: 1.0 W (1% cycle)
ACS	0.1 kg	0.010 W
COMMUNICATIONS	0.5 kg	Tx: 22.3 W (6 min / 6 days) Rx: 0.42 W (10% cycle)
SCIENCE	1.6 kg	1.25 W
DPU	0.3 kg	0.20 W
MECHANICAL		
Solar Cells	0.2	
Thermal Blankets	0.2 kg	
Harnessing	0.2 kg	
Solid rocket, Nutation damper	0.2 kg	
TOTAL	3.93 kg	2.22 W
TOTAL+30%	5.11 kg	2.89 W
Available		3.20 W (From Solar Panels)

Table 3. Launch feasibility

ITEM	WEIGHT (Includes 30% Margin)
Spacecraft (80)	409 kg
Dispenser	151 kg
Total launch capability	560 kg
Taurus XLS (4213) delivers to GTO	593.3 kg
Excess Capacity	33 kg = 8% (Total - Margin)

In addition to the mass estimates of components presented earlier, harnessing at 0.5 lb/ft for wires, and connectors at 20 gr/connector will be required. Wiring thus may weigh ~80 gr (for 320 ft) and connectors 120 gr (6 connectors). Harnessing should be kept to a minimum by using a backplane for most interconnections, and implementing all instrument and ACS functions on the same DPU, resulting in a fully integrated probe rather than independent instruments on a bus. Finally, care should be taken to ensure thermal isolation of the battery and heat dissipation of the transmitter. A passive thermal design is aided by the proposed orbit design that specifically avoids prolonged shadows.

4. Orbit Attainability

Our working hypothesis is a fully autonomous deployer (probe dispenser) that can release and spin up each probe in its ascend to the final orbit. Each probe can be released and spun up by a dispenser-mounted spring. A tentative release mechanism has been studied for a pathfinder mission by Lee et al. [1998]. Probes to be separated only in Z at their apogee should be released at the mean anomaly where their

Table 4. Strawman Mission Cost Estimate

ITEM	COST
Bus components (purchasing/fabrication)	150 K X 80 = 12. M
Instrument fabrication	150 K X 80 = 12. M
Non-recurring engineering cost	10.0 M
Probe calibration/integration/testing	5 M
Ion engine	6 M
Solar panel	1.2 M
Probe dispenser design/fab./integration	5.0 M
Launch & Early Orbit, In-Flight Calibration	1.2 M
Tracking (1 year)	2.5 M
Mission operations	1.5 M
Data Analysis	5 M
SUBTOTAL	61.4 M
Launch (includes launch site operations)	35 M
TOTAL	96.4 M
TOTAL + 30%	125.3 M

orbits intersect; a small ΔV in opposite directions can be imparted by a small solid rocket. This can be done for 10 probes. The remaining 70 probes will not necessitate such a ΔV for orbit change after release.

To raise the probes from GTO to the lowest apogee target orbit (12 R_E) requires a ΔV of 1.1 km/s and monopropellant hydrazine mass equal to 75% of the final (dry) mass. This would necessitate a launch vehicle in the Delta 7920 class (cost $70M) instead of the envisioned Med-Lite class launcher (~$30M). Alternatively, an ion engine results in weight savings and is entirely consistent with the proposed ascend scenario.

The NSTAR solar electric propulsion (SEP) ion engine was recently tested in the DS-1 mission. The engine thrust depends linearly on input power. Input of 2.5 KW results in ~90 mN of thrust. For our purposes 1.25 kW are sufficient, producing 45 mN of thrust. A new type of multijunction solar cells with concentrators designed specifically for use by the NSTAR ion engine has also been tested in DS-1. One "wing" can produce 1.25 kW of power and weighs (including its mounting) 28 kg. Adding 35 kg for the thruster and power processing unit and 10 kg of Xenon fuel (computed out of the rocket equation for the ΔV budget required) we get a total ion engine weight of 73 kg for the SEP propulsion system.

The probe dispenser system can be a six-sided honeycomb structure supporting 6 columns of 13 or 14 probes each. The expected weight of the system's structure is ~20 kg. We assume a 3-axis stabilized dispenser with active attitude control. The control system is used to allow: 1) Good solar panel illumination for efficient orbit raise. 2) Appropriate orientation to maximize the time that the ion engine thrust is along the direction of the required ΔV. 3) Fine-tuning of the orientation at the time of probe release and recovery from momentum change imparted from the release spring. The attitude control will be achieved with a six-nozzle cold gas system. The dry weight of the solenoid valves, pipes, fill and drain port and tank is 8 kg. The fuel required for reorientations is less than 10 kg.

The autonomous dispenser has two antennas, batteries and a DPU for power, thermal, ACS and RF control. A star camera and crude sun sensors are used for ACS functions. Its thermal design is passive. The aforementioned functionality of the dispenser as an autonomous spacecraft entails an additional weight of 5 kg. Thus the total weight of the dispenser excluding the probes, but including a 30% margin is 151 kg.

The Taurus XLS can place a payload in excess of 590 kg to a GTO orbit if launched from Cape Canaveral. Alternatively, the Taurus XLS can be launched from Brazil or from French Guiana at an additional cost on the order of $2M, removing the necessity for a large inclination change by the dispenser. This in turn can reduce the total orbit-raise time since a smaller ΔV is required, but it is not mission critical.

5. Preliminary Cost Estimate

The probe cost estimate is performed on a component-by-component basis. No cost model available was adequate for the probes envisioned because the integration possible for the simple probes envisioned has no equivalence in traditional spacecraft designs. The development cost is a small fraction of the total mission cost.

The bulk of the mission cost is primarily on parts procurement, assembly and testing, which is performed in a traditional fashion. Instrument testing costs can be reduced through careful unit design, and by the use of an automated testing facility (such facilities already exist for magnetometers at UCLA and for plasma instruments at UCB but also at other institutions). The ion engine price is based on the NSTAR cost estimate. The solar panel price reflects the cost of the SCARLET II array developed by AEC-ABLE Engineering, Inc. as quoted by that company. The probe dispenser cost is based on a UCB mechanical design and on experience from consultants from the defense industry who have built multi-probe dispensers before. This includes the integration of the probes and the ion engine on a stack that meets the fairing specifications of the launch vehicle. Ground operations are based on HESSI and FAST Experience. They assume free usage of the 11 meter -diameter NASA tracking station recently procured for HESSI and installed at the UC Berkeley campus. A person-month cost is 10 K in all of the above estimates. The total mission cost, including launch vehicle, and assuming a 30% contingency is $125M, which classifies it in the MIDEX category (capped at $140M).

6. Data Visualization and Reduction

The proposed mission transcends traditional data analysis operations associated with single spacecraft. Visualization of multipoint datasets from many different points in space will be necessary. Inversion techniques to fit sparsely sampled data to a prescribed magnetospheric model are important. Three types of data products should be distributed: 1) Synoptic, three dimensional images of extrapolated pressure, magnetic field strength and plasma flow field profiles will give a first look at the dataset (Figure 3). The first generation of an operational magnetospheric model to be used for magnetic field inversion can be the Tsyganenko [1995] model that requires Solar Wind and Dst input and has specified magnetopause currents. The output should be a time-dependent 3-D model parametrized not to fit the AE index as is now the case, but the probe data instead. The location of the probes superimposed in the images when provided to the community will give instantaneous information on magnetospheric conditions but also on data availability and the extent to which the synoptic images are restricted by measurements. 2) A three dimensional walk through space in a "Virtual Reality" fashion is possible. Much like the HTML language which has recently revolutionized data exchange and communications of two-dimensional information, the VRML language is now on the verge of revolutionizing the exchange of three-dimensional images (http://vrml.wired.com/). Selection of a probe in a hypertext fashion will open up a separate window with time series overview information on a single probe. The user can then request the data from that period, plot the data locally or click on another probe to intercompare data from two points. 3) Raw data will be sent to the user upon request in a fashion employed by the CDHF facility. The user will be able to

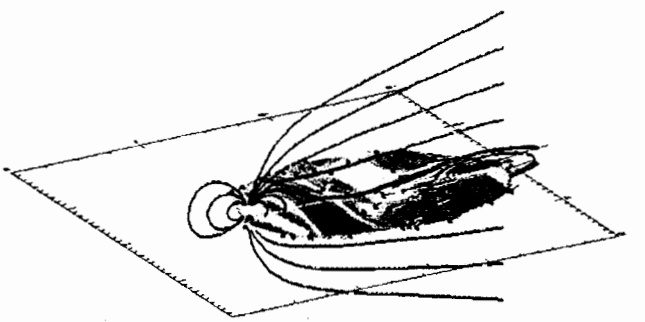

Figure 3. The reconstructed equatorial energy flux density and global magnetic field during the time of a plasmoid formation and its downtail ejection. Probes were run through an MHD simulation of the magnetosphere and the measured parameters were used to reconstruct the equatorial energy flux density. Mapping moments and distribution functions along reconstructed model field lines can produce information within a large volume of the tail.

select events in order to satisfy their analysis needs based on probe position and density of coverage in the synoptic images, or by querying the orbit database, or based on probe conjunctions with a ground station. In that design the mission will be the direct beneficiary of ISTP (http://sscoll.gsfc.nasa.gov/) and CLUSTER (http://wdcc1.bnsc.rl.ac.uk/gbdc) data access and distribution software.

7. Conclusions

The equatorial magnetosphere encompassing the elements controlling the structural stability and the dynamic evolution of the magnetosphere. The drivers of steady-state convection and explosive energy release can be revealed only if the spatial gradients of the plasma pressure, magnetic field, and flow field can be measured. The critical but elusive scale-lengths are primarily in the Y-GSM direction. The mission proposed herein is tailored to answering an array of outstanding questions in the field of magnetotail stability and dynamics, while remaining significantly below the Solar Terrestrial Probe Line budgetary constraints. The science objectives outlined are not only significant but also feasible as a part of a larger, incrementally deployed Constellation mission.

Acknowledgments. This work was supported by CALSPACE grant CS-55-97 and NASA NAGW-5019.

References

Aggson, T. L., et al., Observations of large magnetospheric electric fields during the onset phase of a substorm, J. Geophys. Res., 88, 3981, 1983.

Angelopoulos, V., et al., Characteristics of ion flow in the quiet state of the inner plasma sheet, Geophys. Res. Lett., 20, 1711, 1993.

Angelopoulos, V. et al., Statistical characteristics of bursty bulk flow events, J. Geophys. Res., 99, 21257, 1994.

Angelopoulos, V. et al., Magnetotail flow bursts: association to global magnetospheric circulation, relationship to ionospheric activity and direct evidence for localization, Geophys. Res. Lett., 24, 2271, 1997.

Angelopoulos, V., and H. Spence, Magnetospheric constellation: Past, present, and future, in The Physics of Sun-Earth Plasma and Field Processes, AGU monograph series, Ed. by J. L. Burch, 1998.

Angelopoulos, V., et al., Tracking and operations of constellation microspacecraft, in Science closure and enabling technologies for Constellation class missions, UC Berkeley, Calif., (this volume), 1998.

Ashour-Abdalla, M., et al., Consequences of magnetotail ion dynamics, J. Geophys. Res., 99, 14891, 1994.

Baker, D. N., and R. L. McPherron, Extreme energetic particle decreases near the geostationary orbit: A manifestation of current diversion within the inner plasma sheet, J. Geophys. Res., 95, 6591, 1990.

Baumjohann, W., and G. Paschmann, Determination of the polytropic index in the plasma sheet, Geophys. Res. Lett., 16, 295, 1989.

Baumjohann, W., et al., Average plasma properties in the central plasma sheet, J. Geophys. Res., 94, 6597, 1989.

Baumjohann, W., et al., Characteristics of high-speed ion flows in the plasma sheet, J. Geophys. Res., 95, 3801, 1990.

Berchem, J., et al., Interactive visualization of numerical simulation results: A tool for mission planning and data analysis, in: Visualization techniques in space and atmospheric sciences, E. P. Szuszczewics and J. H. Bredekamp Eds. NASA SP-519, 1995.

Borovsky, J. E., et al., The Earth's plasma sheet as a laboratory for turbulence in high-beta MHD, J. Plasma Phys., 57, 1, 1997.

Delory, G. T., et al., A high science return low-cost Constellation pathfinder, in Science closure and enabling technologies for Constellation class missions, UC Berkeley, Calif., (this volume), 1998.

Ghil, M. and P. Malanotte-Rizzoli, Data assimilation in meteorology and oceanography, Adv. Geophys., 33, 141, 1991.

Goertz, C. K., and W. Baumjohann, On the thermodynamics of the plasma sheet, J. Geophys. Res., 96, 20,991-20,998, 1991.

Huang, C. Y.,et al., Nonadiabatic heating of the central plasma sheet at substorm onset, J. Geophys. Res., 97, 1481-1495, 1992.

Huang, C. Y., et al., Observational determination of the adiabatic index in the quiet time plasma sheet, Geophys. Res. Lett., 16, 563, 1989.

Jacquey, C., et al., Tailward propagating cross-tail current disruption and dynamics of near-Earth tail: A multi-point measurement analysis, Geophys. Res. Lett., 20, 983, 1993.

Kennel, C. F., The Kiruna conjecture: The strong version, in First International Conference on Substorms, ESA SP-335, 599, 1992.

Lee, G. Y., et al., Mechanical considerations of release and spin-up of Constellation microspacecraft, in Science closure and enabling technologies for Constellation class missions, UC Berkeley, Calif., (this volume), 1998.

Lin, N., et al., Multipoint reconnection in the near-Earth magnetotail: CDAW 6 observations of energetic particles and magnetic field, J. Geophys. Res., 96, 19,27, 1991.

Lopez, R. E., and A. T. Y. Lui, A multi-satellite case study of the expansion of a substorm current wedge in the near-Earth magnetotail, J. Geophys. Res., 95, 8009, 1990.

Lui, A. T. Y., Current disruption in the Earth's magnetosphere: Observations and models, J. Geophys. Res., 101, 13067, 1996.

Mauk, B. H., Quantitative modeling of the "Convection Surge" mechanism of ion acceleration, J. Geophys. Res., 13, 423, 1986.

Maynard, N C., et al., Dynamics of the inner magnetosphere near times of substorm onsets, J. Geophys. Res., 101, 7705, 1996.

McComas, D. J., et al., The near-Earth cross-tail current sheet: Detailed ISEE 1 and 2 case studies, J. Geophys. Res., 91, 4287, 1986.

McPherron, R. L., Physical processes producing magnetospheric substorms and magnetic storms, Geomagnetism, 4, 593, 1991.

Nagai, T., Observed magnetic substorm signatures at synchronous altitudes, J. Geophys. Res., 87, 4405, 1982.

Nagai, T., et al., Substorm, tail flows, and plasmoids, Adv. in Space Res., 20, 961, 1997.

Ohtani, S., et al., Radial expansion of the tail current disruption during substorms: A new approach to the substorm onset region, J. Geophys. Res., 97, 3129, 1992.

Pulkkinen, T. I., et al., Modeling the growth phase of a substorm using the Tsyganenko model and multi-spacecraft observations: CDAW-9, Geophys. Res. Lett., 18, 1963, 1991.

Quinn, J. M., and D. J. Southwood, Observations of parallel ion energization in the equatorial region, J. Geophys. Res., 87, 10536, 1982.

Robert, P., et al., GEOS 2 identification of rapidly moving current structures in the equatorial outer magnetosphere during substorms, J. Geophys. Res., 89, 819, 1984.

Rostoker, G., et al., Magnetospheric substorms-definitions and signatures, J. Geophys. Res., 85, 1663, 1980.

Roux, A., et al., Role of the near Earth plasmasheet at substorms, in Magnetospheric Substorms, Geophys. Monogr. Ser., vol. 64, p. 201, AGU, 1991.

Sergeev, V. A., et al., In situ observations of magnetotail reconnection prior to the onset of a small substorm, J. Geophys. Res., in press, 1995.

Sergeev, V. A., et al., Spatial and temporal characteristics of impulsive structure of magnetospheric substorm, J. Geophys. Res., 60, 186-198, 1986.

Shiokawa, K., et al., High-speed ion flow, substorm current wedge, and multiple Pi 2 pulsations, J. Geophys. Res., 103, 4491, 1998.

Spence, H. E., and M. G. Kivelson, Contributions of the low-latitude boundary layer to the finite width magnetotail convection model, J. Geophys. Res., 98, 15487, 1993.

Spence, H. E., et al., The Galileo Earth-1 flyby: Comparison of the finite width tail convection model with observations, 1993 Fall AGU meeting, EOS Trans. 74, 544, 1993.

Stern, D. P., and N. A. Tsyganenko, Uses and limitations of the Tsyganenko magnetic field models, 73, 489, 1992.

Tsyganenko, N. A., Modeling the Earth's magnetic field confined within a realistic magnetopause, J. Geophys. Res., 100, 5599, 1995.

Tsyganenko, N. A., and Usmanov, A. V., Determination of the magnetospheric current system parameters and development of experimental geomagnetic field lines based on data from IMP and HEOS satellites, Plant. Space Sci., 30, 985, 1982.

Yuriev, G. Y., et al., Antenna subsystem solution for Constellation class microspacecraft, in Science closure and enabling technologies for Constellation class missions, UC Berkeley, Calif., (this volume), 1998.

V. Angelopoulos, C. W. Carlson, G. T. Delory, P. Harvey, R. P. Lin, F. S. Mozer, and D. H. Pankow, SSL/UCB, Berkeley, CA 94720-7450, USA (vassilis@ssl.berkeley.edu)

J. Raeder, and C. T. Russell, IGPP/UCLA, Los Angeles, CA 90025. (jraeder@igpp.ucla.edu)